Electron-nuclear double-resonance of titanium in silicon : Si-29 ENDOR

van Wezep, D.A.; van Kemp, R.; Sieverts, E.G.; Ammerlaan, C.A.J.

DOI
10.1103/PhysRevB.32.7129
Publication date
1985

Published in
Physical Review. B, Condensed Matter

Electron-nuclear double resonance of titanium in silicon: ^{29}Si ENDOR

D. A. van Wezep, R. van Kemp, E. G. Sieverts, and C. A. J. Ammerlaan
Natuurkundig Laboratorium der Universiteit van Amsterdam, Valckenierstraat 65, 1018 XE Amsterdam, The Netherlands
(Received 13 June 1985; revised manuscript received 11 October 1985)

The Si-NL29 EPR spectrum, which is associated with the positive charge state of interstitial titanium in silicon, was investigated by electron-nuclear double resonance. Hyperfine-interaction parameters of 17 shells of silicon neighbors, comprised of 214 atoms, could be determined. These parameters are analyzed in a linear combination of atomic orbitals treatment that takes the symmetry properties of the $(t_2)^3$ paramagnetic state into account. This analysis yields a minimum value for the spin density that is transferred from the Ti^+ ion to the surrounding Si atoms. In a tentative assignment of hyperfine tensors to specific lattice sites a spin transfer of at least 40% is derived. This can resolve the apparent contradiction between reduced central-nucleus hyperfine field and absence of ^{29}Si hyperfine interactions in EPR.

I. INTRODUCTION

In comparison to other transition-metal impurities, titanium diffuses relatively slowly into silicon; its diffusion coefficient at 1100 °C is at least 3 orders of magnitude smaller than that of the other metals of the first transition series. Titanium introduces two donor levels in the gap, near $E_v+0.25$ eV and $E_c-0.28$ eV;[1,2] additionally, an acceptor level at $E_c-0.08$ eV has been found.[3] An identification of these levels with $3d^2/3d^3$, $3d^3/3d^4$, and $3d^4/3d^5$, respectively, was suggested by Weber[4] on the basis of the Ludwig-Woodbury model,[5] assuming interstitial solution of titanium in spite of the low diffusion coefficient.

Recently, a new electron-paramagnetic-resonance (EPR) spectrum, labeled NL29, with isotropic $g=1.998\,06\pm0.000\,04$ and spin $S=\frac{3}{2}$, was observed.[6] On the basis of the hyperfine structure and with the use of the Ludwig-Woodbury model, this spectrum could be ascribed to Ti^+ in a $3d^3$ state at an interstitial site of $\bar{4}3m$ symmetry, supporting the identification of deep-level transient-spectroscopy (DLTS) levels. From the observed g shift a large reduction of the spin-orbit—coupling parameter as compared to the free ion could be deduced. At the same time a reduction of the core polarization with respect to the free ion was deduced from the hyperfine interaction with magnetic ^{47}Ti and ^{49}Ti nuclei ($A=15.66\pm0.03$ MHz). These reductions, when interpreted in simple ligand-field theory, would indicate a substantial spin transfer of some 75% to the surrounding silicon lattice. Although such a transfer would not be incompatible with the observed low diffusion coefficient of titanium, such an interpretation is contradicted by the absence of resolved hyperfine interactions of this spin density with magnetic ^{29}Si nuclei in EPR. In order to gain some more insight into this problem we applied electron-nuclear double resonance (ENDOR) to the Ti^+ system. This technique has a resolving power that is 3 orders of magnitude larger than EPR and has proved to yield valuable information concerning the distribution of the spin density over the silicon lattice in a variety of systems like shallow donors,[7,8] radiation defects,[9,10] chalcogenides,[11–13] and, recently, interstitial iron[14] in silicon.

The interpretation of these latter measurements ran into the same difficulties as mentioned for titanium; only 5% of the spin density could be traced back to the six shells of Si neighbors with which hyperfine interactions were measured, while the reduction in core polarization on the central nucleus amounts to 43%, indicating a far larger spin delocalization. This problem has been addressed by Katayama-Yoshida and Zunger,[15] who obtained reasonable agreement between calculated and experimental spin density on the Fe_i^0 nucleus, but found a 29% spin delocalization, at variance with the ENDOR results.

It will be shown in the following that these difficulties for titanium can be resolved in a linear combination of atomic orbitals (LCAO) treatment that takes proper account of the symmetry and spin multiplicity of the paramagnetic state. When applied to the Ti_i^+ ENDOR data this analysis allows much larger amounts of spin transfer than the one-electron treatment of Watkins and Corbett[16] and thus yields results consistent with the covalently delocalized picture. The similar case of Fe_i^0 will be the subject of a separate paper.

II. EXPERIMENTAL PROCEDURE

Floating-zone dislocation-free p-type silicon samples ($20\times2\times2$ mm^3) of various dopings (B, Al, Ga, and In) were rubbed with wet TiO_2 powder and subsequently annealed for 10 d at 1380 °C under an argon atmosphere in a closed ampoule of synthetic quartz. After annealing, samples were allowed to cool to just below red heat at the entrance of the oven and quenched to room temperature from there. The samples were then stored at 77 K until the measurements. In all these samples the Ti^+ EPR resonance could be observed; the best signal (large signal-to-noise ratio, no line broadening due to internal stresses) was obtained from an In-doped sample of initial resistivity 10 Ω cm, containing 0.12×10^{16} In/cm^3, that was there-

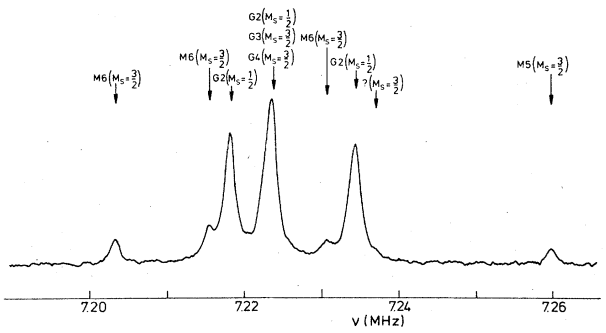

FIG. 1. Recorder trace of the Ti^+ ENDOR spectrum at 4.2 K and $\nu=22.901\,41$ GHz for $B=818.93$ mT, $\mathbf{B}\|[111]$. Labels M5, G2, etc. refer to the hyperfine tensors. The resonance labeled ? forms part of an only partially resolved pattern, the symmetry type of which could not be established.

fore selected for the ENDOR measurements.

These measurements were performed with a superheterodyne spectrometer operating at 23 GHz and adjusted to detect the dispersion part of the EPR signal at an incident microwave power of 1 μW. The magnetic field could be rotated in the $(0\bar{1}1)$ plane of the sample and was modulated at a frequency of 83 Hz. We used a silver-coated epibond cavity; in the thin silver layer on the cylindrical side wall of the cavity a spiral groove was cut, making it suitable as an ENDOR coil.[9] For ENDOR measurements the rf field was square-wave-modulated at 3.3 Hz to allow double phase-sensitive detection of the signal. An example of such a signal is given in Fig. 1. The sample was held at 4.2 K.

III. EXPERIMENTAL RESULTS

Each lattice site around a Ti atom at a T_d interstitial site has a 4.7% probability of being occupied by a ^{29}Si isotope with nuclear spin $I=\frac{1}{2}$. By applying the symmetry operations of the $\bar{4}3m$ symmetry group on such a ^{29}Si atom at a general position in the lattice, a shell of symmetry-related lattice sites is generated. In general, this shell will contain 24 atoms, giving rise to an ENDOR spectrum of $(2S+1)\times 24$ frequency lines for a general direction of the magnetic field B. If the magnetic field is in a $\{011\}$ plane, there are only $(2S+1)\times 12$ resonances (or less if the magnetic field is along a high-symmetry direction). The angular dependence of ENDOR lines originating from such a shell on rotation of the magnetic field in the $(0\bar{1}1)$ plane is shown in Fig. 2(a). Experimentally, resonances from four such shells were found, labeled G1—G4 (G denoting general class). If the initial site is in a $\{011\}$ mirror plane through the central ion, the shell contains only 12 atoms, leading to a reduction of the number of ENDOR lines [Fig. 2(b)]. Eight shells of this symmetry type were found, labeled M1—M8 (M denoting mirror plane). The atoms labeled 3 in Fig. 3 form part of such a shell. If the ^{29}Si atom is on a $\langle 100\rangle$ axis through the central ion, the shell will contain six atoms. The ENDOR pattern of such a $2mm$-symmetry-class shell is also given in Fig. 2; only one such pattern was found, labeled

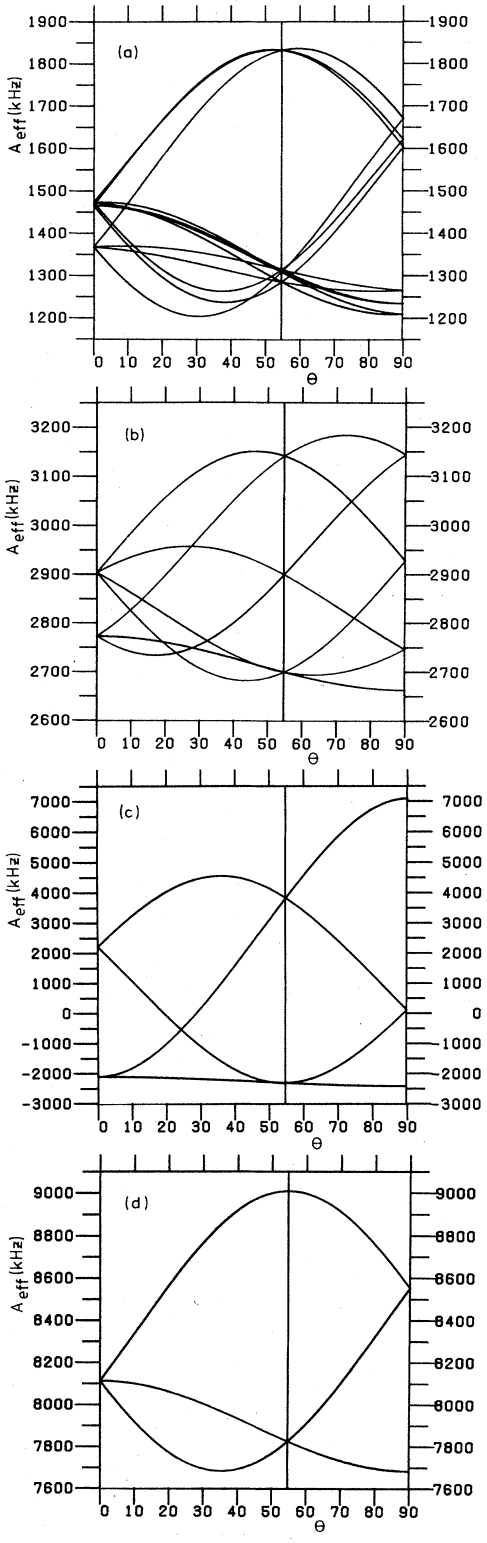

FIG. 2. Angular dependence of the effective hyperfine constant A for the four symmetry types of shells on rotation of the magnetic field in the $(0\bar{1}1)$ plane, shown as examples of (a) a G-class interaction (the pattern is that of the G1 shell), (b) an M-class interaction (the pattern arises from the M1 shell), (c) a $2mm$-class interaction (the pattern is that of the T1 shell), and (d) a 3-class interaction (the pattern arises from the 31 shell).

T1 (T denoting twofold axis). The atoms numbered 2 in Fig. 3 constitute such a shell. If the initial ion is on a ⟨111⟩ axis of threefold rotational symmetry through the central ion, only four symmetry-related sites are generated. Four such shells were found experimentally [Fig. 2(d)], labeled 31—34. Atoms labeled 1 in Fig. 3 constitute a shell of this type. No other types of shells exist in T_d symmetry; the 17 measured shells contain in total a number of 214 Si atoms.

The data were analyzed with the following spin Hamiltonian, containing electronic Zeeman, hyperfine, and nuclear Zeeman interaction terms:

$$\mathcal{H}=g\mu_B\mathbf{B}\cdot\mathbf{S}+\sum_i(\mathbf{S}\cdot\overleftrightarrow{\mathbf{A}}_i\cdot\mathbf{I}_i-g_N\mu_N\mathbf{B}\cdot\mathbf{I}_i)\,, \tag{1}$$

where the parameter i enumerates the lattice sites around the defect. The ENDOR transitions are, to first order, given by

$$h\nu=\Delta E=|\,g_N\mu_N B-\hat{\mathbf{h}}\cdot\overleftrightarrow{\mathbf{A}}\cdot\hat{\mathbf{h}}m_s\,|\,, \tag{2}$$

with $\hat{\mathbf{h}}$ a unit vector along the magnetic field $\mathbf{B}$. The ENDOR spectrum is thus seen to be symmetric around the nuclear Zeeman frequency $g_N\mu_N B/h$. Therefore only transitions above the nuclear Zeeman frequency needed to be measured. It was not always possible to observe the transitions in both the $|m_s|=\frac{1}{2}$ and $|m_s|=\frac{3}{2}$ multiplets; due to severe overlapping of ENDOR patterns in the region close to the nuclear Zeeman frequency, the determination of the $|m_s|=\frac{1}{2}$ transitions was often obstructed in that part of the spectrum. On the other end of the ENDOR spectrum, the $|m_s|=\frac{3}{2}$ resonances were very weak and therefore not always used in the analysis. The complete ENDOR spectrum of all measured shells is given in Fig. 4.

We obtained a satisfactory least-squares fit to the ENDOR data in a computer diagonalization of the Hamiltonian (1), keeping the electronic g value fixed at $g=1.998\,06$ (Ref. 6) and the nuclear g value at $g_N=-1.1097$.[17] The results are summarized in Table I, where it is also indicated which transitions were used in

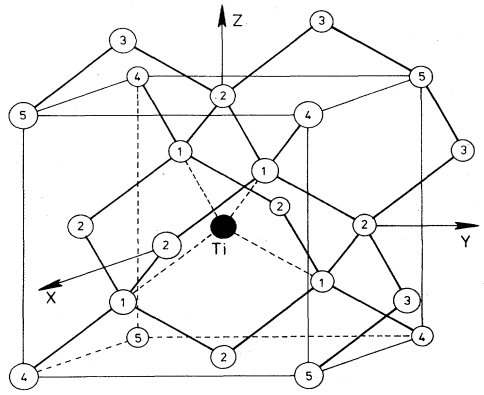

FIG. 3. The Ti interstitial (black sphere) surrounded by Si atoms. This figure also shows our choice of coordinate system, on which the Cartesian hyperfine tensors and directions of eigenvectors of Table I are defined.

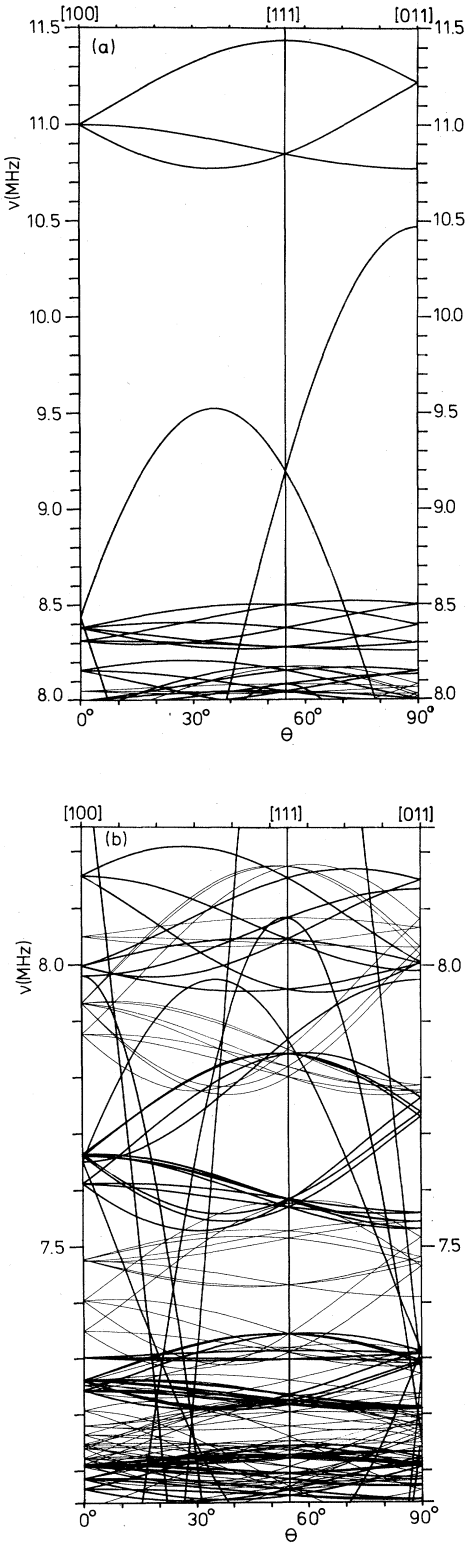

FIG. 4. The complete angular dependence of resolved ENDOR resonances on rotation of the magnetic field in the $(0\bar{1}1)$ plane. The thick lines designate the ENDOR transitions in the $|m_s|=\frac{1}{2}$ multiplet, the thin lines those in the $|m_s|=\frac{3}{2}$ multiplet.

TABLE I. Parameters and orientations of hyperfine tensors of ^{29}Si neighbors of Si:Ti$^+$ (in kHz). Experimental uncertainty is ±0.4 kHz.

Shell	$\lvert m_s \rvert$	$\vec{\vec{A}}$			i	A_i	$\mathbf{n}_i$
31	$\frac{1}{2}$	8123.6	441.6	441.6	1	9006.9	(−0.577, −0.577, −0.577)
		441.6	8123.6	441.6	2	7682.0	(+0.408, −0.816, +0.408)
		441.6	441.6	8123.6	3	7682.0	(+0.707, +0.000, −0.707)
32	$\frac{1}{2}$	1416.9	−678.2	−678.2	1	60.5	(−0.577, −0.577, −0.577)
		−678.2	1416.9	−678.2	2	2095.1	(+0.408, −0.816, +0.408)
		−678.2	−678.2	1416.9	3	2095.1	(+0.707, +0.000, −0.707)
33	$\frac{1}{2}, \frac{3}{2}$	748.5	11.5	11.5	1	771.5	(−0.577, −0.577, −0.577)
		11.5	748.5	11.5	2	737.0	(+0.408, −0.816, +0.408)
		11.5	11.5	748.5	3	737.0	(+0.707, +0.000, −0.707)
34	$\frac{3}{2}$	129.5	−18.2	−18.2	1	93.1	(−0.577, −0.577, −0.577)
		−18.2	129.5	−18.2	2	147.6	(+0.408, −0.816, +0.408)
		−18.2	−18.2	129.5	3	147.6	(+0.707, +0.000, −0.707)
T1	$\frac{1}{2}$	2333.1	4751.6	0.0	1	7084.7	(−0.707, −0.707, +0.000)
		4751.6	2333.1	0.0	2	−2418.6	(−0.707, +0.707, +0.000)
		0.0	0.0	−2108.9	3	−2108.9	(+0.000, +0.000, +1.000)
M1	$\frac{1}{2}$	2902.1	240.5	90.5	1	2661.5	(−0.707, +0.707, +0.000)
		240.5	2902.1	90.5	2	3182.4	(−0.675, −0.675, −0.297)
		90.5	90.5	2771.3	3	2731.5	(+0.210, +0.210, −0.955)
M2	$\frac{1}{2}$	2139.9	15.0	147.4	1	2124.9	(−0.707, +0.707, +0.000)
		15.0	2139.9	147.4	2	2563.7	(+0.321, +0.321, +0.891)
		147.4	147.4	2457.3	3	2048.6	(−0.630, −0.630, +0.454)
M3	$\frac{1}{2}, \frac{3}{2}$	366.4	44.9	3.3	1	321.6	(−0.707, +0.707, +0.000)
		44.9	366.4	3.3	2	411.8	(−0.704, −0.704, −0.099)
		3.3	3.3	365.0	3	364.5	(−0.070, −0.070, +0.995)
M4	$\frac{1}{2}, \frac{3}{2}$	316.9	74.9	58.6	1	242.0	(−0.707, +0.707, +0.000)
		74.9	316.9	58.6	2	435.9	(−0.624, −0.624, −0.470)
		58.6	58.6	280.6	3	236.4	(+0.333, +0.333, −0.882)
M5	$\frac{3}{2}$	220.7	36.8	−14.6	1	183.9	(−0.707, +0.707, +0.000)
		36.8	220.7	−14.6	2	265.1	(−0.663, −0.663, +0.346)
		−14.6	−14.6	209.2	3	201.6	(+0.245, +0.245, +0.938)
M6	$\frac{3}{2}$	168.7	0.6	−13.1	1	168.1	(−0.707, +0.707, +0.000)
		0.6	168.7	−13.1	2	222.9	(−0.231, −0.231, +0.945)
		−13.1	−13.1	216.6	3	163.0	(−0.668, −0.668, −0.326)
M7	$\frac{3}{2}$	70.5	20.6	24.1	1	49.9	(−0.707, +0.707, +0.000)
		20.6	70.5	24.1	2	197.4	(−0.216, −0.216, −0.952)
		24.1	24.1	186.5	3	80.2	(+0.673, +0.673, −0.305)
M8	$\frac{3}{2}$	119.9	22.5	14.7	1	97.3	(−0.707, +0.707, +0.000)
		22.5	119.9	14.7	2	151.9	(+0.644, +0.644, +0.414)
		14.7	14.7	106.2	3	96.8	(−0.293, −0.293, +0.910)
G1	$\frac{1}{2}$	1471.1	−203.1	−185.0	1	1834.6	(+0.603, −0.615, −0.509)
		−203.1	1464.4	206.6	2	1268.0	(+0.774, +0.605, +0.187)
		−185.0	206.6	1366.1	3	1199.0	(+0.193, −0.507, +0.840)

TABLE I. (*Continued*).

Shell	$\lvert m_s \rvert$	$\overleftrightarrow{A}$			i	A_i	$\mathbf{n}_i$
G2	$\frac{1}{2},\frac{3}{2}$	631.6	−76.8	−85.9	1	834.2	(+0.494, −0.606, −0.623)
		−76.8	667.7	101.0	2	572.1	(−0.597, −0.758, +0.264)
		−85.9	101.0	667.9	3	561.0	(−0.632, +0.242, −0.736)
G3	$\frac{3}{2}$	157.8	−27.9	−23.4	1	198.7	(+0.664, −0.555, −0.501)
		−27.9	146.8	20.6	2	127.2	(−0.541, +0.106, −0.835)
		−23.4	20.6	144.9	3	123.6	(−0.516, −0.825, +0.229)
G4	$\frac{3}{2}$	141.6	−40.2	−28.6	1	198.6	(+0.654, −0.588, −0.476)
		−40.2	130.1	29.4	2	102.2	(−0.596, −0.012, −0.803)
		−28.6	29.4	123.0	3	93.9	(−0.467, −0.809, +0.358)

the fits. The tensors and directions of eigenvectors in this table are defined in the coordinate system of Fig. 3 and valid for the following:

(1) The atom on the [111] axis for shells 31–34.
(2) One of the two atoms on the [001] axis for T1, since no unique assignment of the hyperfine tensor to one of these two atoms can be made.
(3) One of the two atoms in the $(\bar{1}10)$ mirror plane, for shells M1–M8 (as for T1).
(4) One of the 24 atoms in the low-symmetry shells G1–G4 (as for T and M shells).

Data for atoms in the shells, other than just specified, can be obtained by applying the appropriate symmetry transformations.

Typical widths of the resonances were 2–3 kHz full width at half maximum (FWHM), allowing line positions to be determined with an accuracy better than 0.4 kHz. The deviations of calculated ENDOR frequencies from experimental values were generally less than this value.

IV. DISCUSSION

The hyperfine-interaction tensor is usually split into two parts, $\overleftrightarrow{A}=a\overleftrightarrow{1}+\overleftrightarrow{B}$, where a is the isotropic part of the hyperfine tensor $a=(\mathrm{Tr}\overleftrightarrow{A})/3$ and $\overleftrightarrow{B}$ a symmetric traceless tensor. Both parts have their interpretation in terms of the defect wave function; a is related to the wave function through the Fermi-contact interaction,

$$a=\tfrac{2}{3}\mu_0 g\mu_B g_N\mu_N \lvert\Psi(0)\rvert^2 , \tag{3}$$

where $\lvert\Psi(0)\rvert^2$ is the probability density of the paramagnetic electrons on the nucleus involved. The dipole-dipole interaction between the magnetic moments of electron density and nucleus is responsible for the anisotropic part of the tensor:

$$B_{ij}=\frac{\mu_0}{4\pi}g\mu_B g_N\mu_N\left\langle\Psi\left|\frac{3x_ix_j}{r^5}-\frac{\delta_{ij}}{r^3}\right|\Psi\right\rangle , \tag{4}$$

where Ψ is the electronic wave function and $x_i,x_j=x,y,z$.

Following Owen and Thornley,[18] we will describe the wave function of the paramagnetic state by taking linear combinations of $3s$ and $3p$ orbitals of the surrounding silicon lattice that transform as the t_2 irreducible representation of the $\bar{4}3m$-symmetry point group, and admix these to the d_{xy}, d_{yz}, and d_{zx} orbitals of the same t_2 representation that are supposed to make up the paramagnetic state.[5] These combinations are found with the use of projection operators, a procedure outlined, e.g., by Di Bartolo,[19] whose terminology we will use in the following. For the 3-class shells we obtain

$$\Psi_{xy}=\alpha d_{xy}+\tfrac{1}{2}\beta_i(s_1-s_2-s_3+s_4)+\tfrac{1}{2}\gamma_i(\sigma_1-\sigma_2-\sigma_3+\sigma_4)+\tfrac{1}{4}\delta_i[(-\pi_{1x}+\pi_{2x}+\pi_{3x}-\pi_{4x})+\sqrt{3}(\pi_{1y}-\pi_{2y}-\pi_{3y}+\pi_{4y})] ,$$
$$\Psi_{yz}=\alpha d_{yz}+\tfrac{1}{2}\beta_i(s_1-s_2+s_3-s_4)+\tfrac{1}{2}\gamma_i(\sigma_1-\sigma_2+\sigma_3-\sigma_4)+\tfrac{1}{4}\delta_i[(-\pi_{1x}+\pi_{2x}-\pi_{3x}+\pi_{4x})-\sqrt{3}(\pi_{1y}-\pi_{2y}+\pi_{3y}-\pi_{4y})] .$$
$$\Psi_{zx}=\alpha d_{zx}+\tfrac{1}{2}\beta_i(s_1+s_2-s_3-s_4)+\tfrac{1}{2}\gamma_i(\sigma_1+\sigma_2-\sigma_3-\sigma_4)+\tfrac{1}{2}\delta_i[(\pi_{1x}+\pi_{2x}-\pi_{3x}-\pi_{4x})] . \tag{5}$$

The numbers 1, 2, 3, and 4 refer to the ligands at the positions nnn, $\bar{n}n\bar{n}$, $n\,\bar{n}\,\bar{n}$, and $\bar{n}\,\bar{n}\,n$ (n is an integer), respectively, the index i enumerates the 3-class shells, and α, β_i, γ_i, and δ_i are parameters to be determined by experiment. The orbitals designated by σ are p orbitals on the ligand, taken to point in the direction of the central ion, while the π_{1x} and π_{1y} are taken to point along the $[1\bar{2}1]$ and $[10\bar{1}]$ directions, respectively. The orientations of the orbitals on the other ligands are obtained by C_2 rotations about the x, y, and z axes [Fig. 5(a)]. The wave function is only normalized when the ligand contributions from *all* shells are added; α^2 is then the spin density on the central nucleus.

For $d^3(t_2^3)$ the orbital magnetic moment is quenched and the ground-state wave function is then a single determinant,

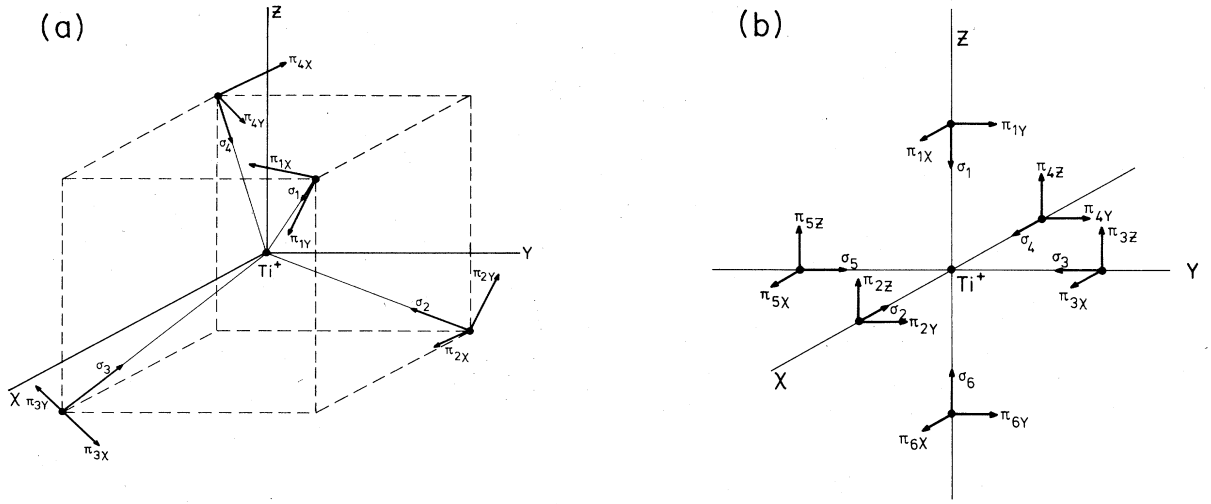

FIG. 5. Orientations of σ and π orbitals on atoms constituting (a) a 3-class shell and (b) a $2mm$-class shell.

$$\{\Psi_{xy}(\uparrow)\Psi_{yz}(\uparrow)\Psi_{zx}(\uparrow)\}\ .$$

In this case it is permissible to add up the separate contributions to the hyperfine structure from the individual singly occupied orbitals.[18] In deriving the matrix elements of (3) and (4) we make the usual LCAO approximation and neglect contributions to $\vec{\vec{B}}$ from atoms on other lattice sites than the one considered, except those from the central ion, which are calculated in the point-dipole approximation. For a p orbital of the form $\Psi_p = x_1 f(r)$ on atom 1 ($x_1 = x,y,z$), we obtain

$$\vec{\vec{B}} = \frac{1}{2S}\left(\tfrac{3}{4}\gamma_i^2 - \tfrac{3}{8}\delta_i^2\right)\begin{bmatrix} -b & & \\ & -b & \\ & & 2b \end{bmatrix} + \frac{1}{2S}3\alpha^2\begin{bmatrix} -b_{dd} & & \\ & -b_{dd} & \\ & & 2b_{dd} \end{bmatrix}, \tag{6}$$

with

$$b = \frac{2}{5}\frac{\mu_0}{4\pi} g\mu_B g_N \mu_N \langle r^{-3}\rangle_p$$

and

$$b_{dd} = \frac{\mu_0}{4\pi} g\mu_B g_N \mu_N R^{-3}$$

(R denotes Ti-^{29}Si distance). The isotropic part is given by

$$a = \frac{1}{2S}\frac{3}{4}\beta_i^2\frac{2}{3}\mu_0 g\mu_B g_N\mu_N |s_1(0)|^2 = \frac{1}{2S}\frac{3}{4}\beta_i^2 a_0\ . \tag{7}$$

The factor $1/2S$ allows for the fact that our results are expressed in the total spin $\mathbf{S}$ ($S=\frac{3}{2}$). Due to our choice of coordinates this tensor is on principal axes and may be conveniently compared to experiment.

In $S=\frac{1}{2}$ systems these tensors are given by $A_{xx}=A_{yy}=a'-b'$ and $A_{zz}=a'+2b'$, in which $a'=\eta^2\alpha^2 a_0$ and $b'=\eta^2\beta^2 b$. The spin density on the atom concerned is then given by η^2, while the relative distribution over s and p orbitals is given by α^2 and β^2, respectively.[16] In this analysis a' and b' are required to have the same sign, a limitation which is no longer valid if this analysis is applied to higher-spin systems, as can be seen by inspection of (6). In a situation where the spin density in the π orbitals exceeds that in the σ orbitals by at least a factor of 2, $\frac{3}{4}\gamma_i^2 - \frac{3}{8}\delta_i^2$ will be negative, thus causing a' and b' to be of opposite sign (neglecting distant dipole-dipole interactions for simplicity). Experimentally, this situation occurs, e.g., for tensor 32 for all values of α, independent of the assignment to a specific atom. As an example, one can consider in (5) such combinations of σ and π bonds on the nearest-neighbor atoms that their directions coincide with the lattice bonds between the atoms 1 and 2 in Fig. 3. In this case, $\delta_1 = 2\sqrt{2}\gamma_1$, so that

$$\tfrac{3}{4}\gamma_1^2 - \tfrac{3}{8}\delta_1^2 = -2.25\gamma_1^2 = 2S\frac{b'}{b}\ .$$

This also serves as an illustration of the enhanced spin transfer in comparison to the spin density that would be derived from a one-electron treatment.

From (6) and (7) it is obvious that γ_i^2 and δ_i^2 cannot be determined separately from experiment and, consequently, the transferred spin density to a shell $\beta_i^2+\gamma_i^2+\delta_i^2$ cannot be obtained from the data. It is possible, however, to obtain an estimate of the minimum spin density (as a function of α^2) that is transferred to a shell of silicon neighbors (MTSD) by setting either γ_i^2 or δ_i^2 equal to zero, depending on the sign of B_{xx}, and using the values for $|s_1(0)|^2$ and $\langle r^{-3}\rangle_p$.[20]

In the case of a $2mm$-class shell we obtain the following symmetry orbitals:

$$\Psi_{xy}=\alpha d_{xy}+\frac{1}{\sqrt{2}}\beta(s_1-s_6)+\frac{1}{\sqrt{2}}\gamma(\sigma_1-\sigma_6)+\tfrac{1}{2}\delta(\pi_{2z}+\pi_{3z}+\pi_{4z}+\pi_{5z})+\tfrac{1}{2}\epsilon(\pi_{2y}+\pi_{3x}-\pi_{4y}-\pi_{5x}) ,$$

$$\Psi_{yz}=\alpha d_{yz}+\frac{1}{\sqrt{2}}\beta(s_2-s_4)+\frac{1}{\sqrt{2}}\gamma(\sigma_2-\sigma_4)+\tfrac{1}{2}\delta(\pi_{1x}+\pi_{3x}+\pi_{5x}+\pi_{6x})+\tfrac{1}{2}\epsilon(\pi_{1y}+\pi_{3z}-\pi_{5z}-\pi_{6y}) , \quad (8)$$

$$\Psi_{zx}=\alpha d_{zx}+\frac{1}{\sqrt{2}}\beta(s_3-s_5)+\frac{1}{\sqrt{2}}\gamma(\sigma_3-\sigma_5)+\tfrac{1}{2}\delta(\pi_{1y}+\pi_{2y}+\pi_{4y}+\pi_{6y})+\tfrac{1}{2}\epsilon(\pi_{1x}+\pi_{2z}-\pi_{4z}-\pi_{6x}) .$$

The numbers 1–6 refer to the following atoms: $(0,0,2n)$, $(2n,0,0)$, $(0,2n,0)$, $(-2n,0,0)$, $(0,-2n,0)$, and $(0,0-2n)$. Again, σ designates a p orbital on a ligand, pointing in the direction of the central ion; the π orbitals are along the positive x, y, or z directions for all atoms [Fig. 5(b)]. This choice yields the following hyperfine tensor components of atom 1 on xyz coordinates,

$$B_{xx}=B_{yy}=\frac{1}{2S}[\tfrac{1}{4}(\delta^2+\epsilon^2-2\gamma^2)b-3\alpha^2 b_{dd}] ,$$

$$B_{zz}=-\frac{2}{2S}[\tfrac{1}{4}(\delta^2+\epsilon^2-2\gamma^2)b-3\alpha^2 b_{dd}] , \quad (9)$$

$$B_{xy}=B_{yx}=\frac{1}{2S}\frac{3}{2}\delta\epsilon b ,$$

$$B_{xz}=B_{zx}=B_{yz}=B_{zy}=0 ,$$

and the isotropic part,

$$a=\frac{1}{2S}\frac{1}{2}\beta^2\frac{2}{3}\mu_0 g\mu_B g_N\mu_N |s_1(0)|^2 . \quad (10)$$

By inspection of (9) and (10) it can be seen that the spin density in the $\sigma(\gamma^2)$ and $\pi(\delta^2,\epsilon^2)$ orbitals can not be obtained separately from the data; neither can the total spin density in the p orbitals in a shell $\gamma^2+\delta^2+\epsilon^2$ be determined. As in the case of the 3-class tensors, only a minimum value for the spin transfer can be extracted from the data.

Similarly, it is possible to derive (rather lengthy) expressions for the symmetry orbitals and hyperfine tensors of M- and G-class atoms. For the M-class tensors the symmetry orbitals contain five independent parameters for the admixture of σ and π orbitals; in the case of G-class tensors there are even nine such parameters. Again, the sum of all admixed amounts can not be related directly to the experimental data, so that only a minimum of the transferred spin density can be determined. For this purpose the expressions for the hyperfine tensors are conveniently solved in the $\sigma\pi_x\pi_y$-coordinate system, necessitating, however, the transformation of the experimental tensor to this coordinate system and thus the assignment of the experimental tensor to a specific shell (atom). For the M-class shells this assignment was accomplished by evaluating the angle between the largest eigenvector and possible lattice vectors to the atoms in the $(\bar{1}10)$ plane. It was found that an assignment could be made where the principal directions of the largest principal values of all eight M tensors fell well within 10° from lattice vectors to sites in the eleven closest M-type shells (Table II and Fig. 6). This corresponds to a picture in which transfer to σ orbitals and/or distant dipole-dipole interaction predominate(s) the transfer to π orbitals. Isotropic and anisotropic hyperfine interactions of subsequent shells roughly decrease with distance to the central nucleus in this assignment.

In case of the G-class tensors the same procedure could not be followed, due to the fact that all these tensors are approximately ⟨111⟩-axial. Here we choose rather arbitrarily the nearest shell to have the largest isotropic hyperfine interaction. Since we cannot discriminate which tensor belongs to which specific site in this case, we calculated the MTSD of the tensors G1–G4 for all 24 atoms in a shell as a function of α^2 and choose the smallest MTSD to be *the* MTSD.

In order to take into account the distant dipole-dipole interaction, we also have to assign the 3-class tensors to specific sites in order to obtain an estimate for the MTSD as a function of α^2; again, we assigned the tensor with the largest isotropic hyperfine interaction to the nearest shell. Assigning the tensor with the largest anisotropic hyperfine interaction to the nearest shell would be equally well defendable, but yields larger MTSD values. Since it is our aim to establish a minimum for the spin transfer to all measured shells, we will not pursue this latter identification. The complete assignment is summarized in Table II; for convenience we add a list of lattice sites around the in-

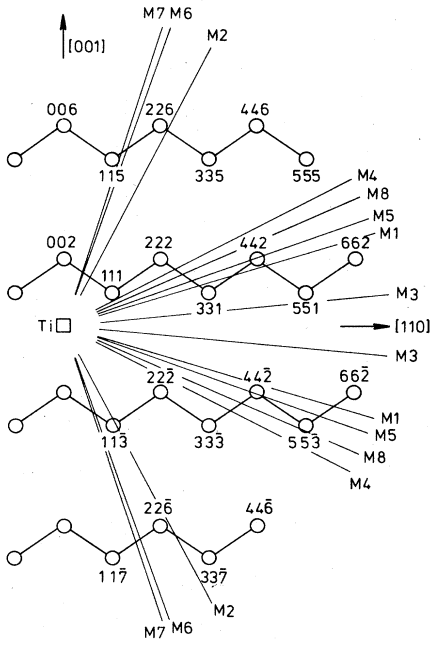

FIG. 6. The cross section of the $(\bar{1}10)$ plane with the Ti interstitial. Indicated by lines are the principal directions of all measured M-class tensors with the largest principal value.

TABLE II. Assignment of experimental tensors to atomic sites around the Ti^+ interstitial and angles between principal axis of largest eigenvalue and lattice vector or the $[1\,\bar{1}\,\bar{1}]$ direction.

Tensor	Atom *lmn*	Axis			Angle with [*lmn*]	Angle with $[1\,\bar{1}\,\bar{1}]$
31	111					
32	222 or $\bar{2}\bar{2}\bar{2}$					
33	$\bar{2}\bar{2}\bar{2}$ or 222					
34	$\bar{3}\bar{3}\bar{3}$					
T1	002 or $00\bar{2}$					
M1	331	(−0.675,	−0.675,	−0.297)	4.0	
M2	$\bar{1}\bar{1}3$	(0.321,	0.321,	0.891)	1.8	
M3	551	(−0.704,	−0.704,	−0.099)	2.4	
M4	442	(−0.624,	−0.624,	−0.470)	8.6	
M5	$44\bar{2}$	(−0.663,	−0.663,	0.346)	0.8	
M6	$22\bar{6}$	(−0.231,	−0.231,	0.945)	6.2	
M7	115	(−0.216,	−0.216,	−0.952)	2.0	
M8	$\bar{5}\bar{5}3$	(0.644,	0.644,	0.414)	1.5	
G1	$\bar{2}40$ or $2\bar{4}0$	(0.603,	−0.615,	−0.509)		4.7
G2	$\bar{5}31$	(0.494,	−0.606,	−0.623)		5.7
G3	$\bar{4}60$ or $4\bar{6}0$	(0.664,	−0.555,	−0.501)		6.7
G4	$\alpha^2<0.25$: $71\bar{3}$ $\alpha^2>0.25$: $1\bar{3}\bar{7}$	(0.654,	−0.588,	−0.476)		7.3

TABLE III. Shells of lattice sites around the T_d interstitial position in silicon. The shells marked with an asterisk (*) show resolved hyperfine interactions in the assignment of Table II.

Shell	Type	Position	Sites	Distance (Å)
1*	3*a*	111	4	2.35
2*	T*a*	200	6	2.71
3*	M*a*	$\bar{3}\bar{1}\bar{1}$	12	4.50
4*	3*b*	222	4	4.70
5*	3*c*	$\bar{2}\bar{2}\bar{2}$	4	4.70
6*	M*b*	331	12	5.91
7*	G*a*	420	24	6.07
8*	3*d*	333	4	7.05
9*	M*c*	511	12	7.05
10*	G*b*	$\bar{5}\bar{3}\bar{1}$	24	8.03
11	T*b*	600	6	8.14
12*	M*d*	442	12	8.14
13*	M*e*	$\bar{4}\bar{4}\bar{2}$	12	8.14
14	M*f*	533	12	8.90
15	M*g*	622	12	9.00
16*	M*h*	$\bar{6}\bar{2}\bar{2}$	12	9.00
17*	M*i*	551	12	9.69
18	M*j*	$\bar{7}\bar{1}\bar{1}$	12	9.69
19*	G*c*	640	24	9.78
20*	M*k*	$\bar{5}\bar{5}\bar{3}$	12	10.42
21*	G*d*	731	24	10.42
22	M*l*	$\bar{7}\bar{3}\bar{3}$	12	11.11
23	M*m*	644	12	11.19
24	M*n*	$\bar{6}\bar{4}\bar{4}$	12	11.19
25	G*e*	820	24	11.19

TABLE IV. Isotropic hyperfine parameters of ^{29}Si neighbors of $Si{:}Ti^+$ (in kHz) and derived spin densities β_i^2 in *s* orbitals per shell (in %).

Shell	*a* (kHz)	β_i^2 (%)
31	8123.6	0.71
32	1416.9	0.12
33	748.5	0.07
34	129.4	0.01
T1	852.4	0.11
M1	2858.4	0.75
M2	2245.7	0.59
M3	366.0	0.10
M4	304.8	0.08
M5	216.9	0.06
M6	184.7	0.05
M7	109.2	0.03
M8	115.3	0.03
G1	1433.9	0.75
G2	655.8	0.34
G3	149.8	0.08
G4	131.6	0.07

terstitial Ti ion (Table III). It should be stressed here that this assignment is a tentative one. The estimate for the MTSD, however, is not altered dramatically if another assignment is chosen. The spin densities derived from the isotropic part of the hyperfine-interaction tensors are collected in Table IV. Together with the (minimum) contributions from the anisotropic part of the hyperfine tensors, MTSD values as a function of α^2 result. These are plotted in Fig. 7. The connection between transferred and Ti-localized spin density is represented by the dashed line in Fig. 7(d); below the point where this line and total MTSD(α^2) intersect ($\alpha^2 \leqq 0.62$), we obtain consistent results; above this point the normalization condition is violated and this region is therefore unphysical. It follows that the spin transfer to the surrounding silicon lattice must be at least 38%.

The MTSD from M- and G-class shells decreases as a function of α^2 as expected, since part of the anisotropy of

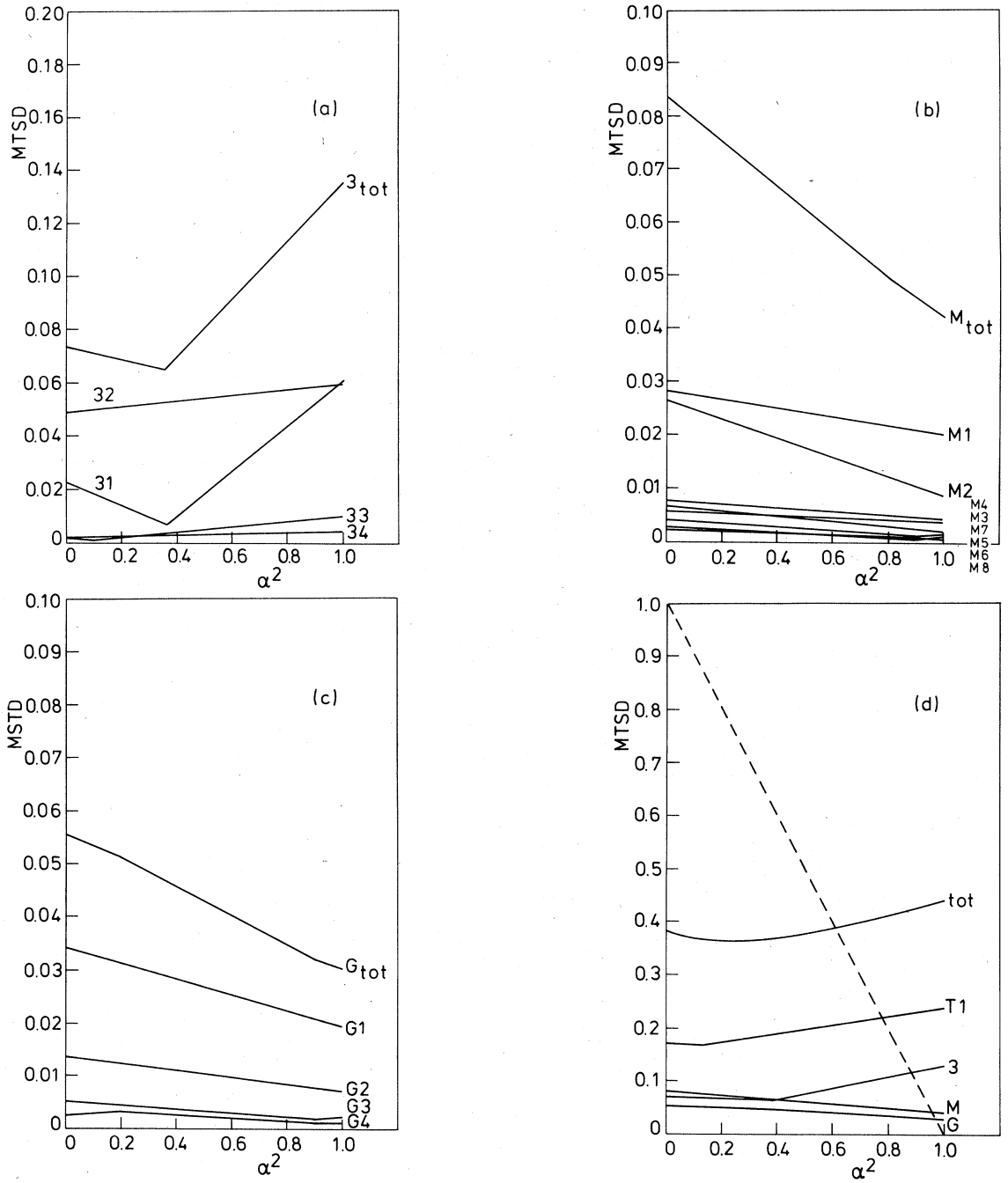

FIG. 7. Minimum transferred spin densities to the lattice versus the spin localization α^2 on the Ti^+ ion as obtained from the hyperfine-interaction tensors in the assignment of Table II. (a) 3-class shells, (b) M-class shells, (c) G-class shells, and (d) total over all shells. The connection between transferred and Ti localized spin density is represented by the dashed line.

these tensors must be due to distant dipole-dipole interaction, necessitating the presence of less spin density on a ^{29}Si nucleus. For the 3- and $2mm$-class shells, however, the MTSD falls first and increases next with increasing α^2. This is caused by the large correction of the distant dipole-dipole interaction, which changes the sign of B_{xx}; in order to maintain consistency with sign and magnitude of the experimental tensors it is then necessary to introduce more spin density in the π orbitals.

That the transfer to π orbitals may be quite significant follows from the fact that T1 is approximately $\langle 011 \rangle$-axial, while the ^{29}Si atom has the Ti ion in a $\langle 100 \rangle$ direction. A large spin density in the σ orbital and/or large dipole-dipole interactions with the central ion would tend to make this tensor axial around a $\langle 100 \rangle$ direction. This observation therefore forms a strong indication that the transfer of spin density to π orbitals of atoms in the second shell is the mechanism determining the hyperfine tensor T1. In this context it should be realized that transfer of spin density from d_{xy},d_{yz},d_{zx} orbitals of a central ion A to σ orbitals of ligand B atoms in an AB_6 complex of $m3m$ point-group symmetry is forbidden. As the six atoms in a $2mm$-class shell bear a close resemblance to such an AB_6 system, it is not unlikely that most of the transferred spin density will be found in the π orbitals; the MTSD of some 20% derived from T1 may therefore be a good indication of the factual spin density in the second-neighbor shell. In the case of the 3-class tensors such an analysis is not fruitful, since both σ and π transfer are allowed in an AB_4 complex, which is itself of $\bar{4}3m$ symmetry. The spin transfer to such shells may therefore be severely underestimated. The real spin density for M- and G-class tensors may for similar reasons be appreciably higher than the derived MTSD on these shells.

The observed reduction in core polarization [though not as high as estimated in Ref. 6, where we erroneously omitted a factor $1/2S$] of some 75% for Ti^{+} is therefore not inconsistent with the hyperfine structure as measured in ENDOR, and constitutes a strong indication that the factual spin transfer to the lattice is indeed of this order. We must be careful with the conclusion that the transferred spin density is 75%, however, since it is based on the assumption that the central-ion hyperfine-interaction parameter is entirely determined by core polarization;[6] a small residual spin density in the $4s$ orbital could alter this estimate considerably. The ^{29}Si ENDOR thus sets a lower limit of 40% to the spin transfer, while the ^{47}Ti hyperfine interaction sets an upper limit of 75%.

A similar treatment was applied to the case of Fe_i^0, where the two paramagnetic electrons are in the e state,[5] for which symmetry orbitals and hyperfine tensors were also derived. These expressions will be published in a forthcoming paper.

V. CONCLUSIONS

The measured perturbation of the titanium interstitial extends over 214 Si atoms in 17 symmetry shells. This indicates a substantial spin transfer to the lattice, consistent with the observed reductions in spin-orbit—coupling parameter and impurity hyperfine field. The absence of resolved hyperfine interactions of this spin density with magnetic ^{29}Si nuclei in EPR can be explained in a LCAO treatment that takes symmetry properties and spin multiplicity of the paramagnetic t_2 state into account: It turns out that the spin density in π orbitals has an opposing effect on the hyperfine-interaction tensor as compared to the distant dipole-dipole interaction with the central nucleus and the spin density in the σ orbitals. As a result only a minimum transferred spin density of $\approx 40\%$ can be obtained from the Ti_i^{+} ENDOR data.

ACKNOWLEDGMENTS

This work received financial support from the Netherlands Foundation for Fundamental Research of Matter (FOM).

[1] J. W. Chen, A. G. Milnes, and A. Rohatgi, Solid State Electron. **22**, 801 (1979).
[2] A. C. Wang and C. T. Sah, J. Appl. Phys. **54**, 1021 (1984).
[3] K. Graff and H. Pieper, in *Semiconductor Silicon 1981,* edited by H. R. Huff, R. J. Kriegler, and Y. Takeishi (The Electrochemical Society, Pennington, N.J., 1981), p. 331.
[4] E. R. Weber, Appl. Phys. A **30**, 1 (1983).
[5] G. W. Ludwig and H. H. Woodbury, in *Solid State Physics,* edited by H. Ehrenreich, F. Seitz, and D. Turnbull (Academic, New York, 1962), Vol. 13, p. 223.
[6] D. A. van Wezep and C. A. J. Ammerlaan, J. Electron Mater. **14a**, 863 (1985).
[7] G. Feher, Phys. Rev. **114**, 1219 (1959).
[8] E. B. Hale and R. L. Mieher, Phys. Rev. **184**, 739 (1969).
[9] J. G. de Wit, E. G. Sieverts, and C. A. J. Ammerlaan, Phys. Rev. B **14**, 3494 (1976).
[10] E. G. Sieverts, S. H. Muller, and C. A. J. Ammerlaan, Phys. Rev. B **18**, 6834 (1978).
[11] G. W. Ludwig, Phys. Rev. **137**, A1520 (1965).
[12] J. R. Niklas and J. M. Spaeth, Solid State Commun. **46**, 121 (1983).
[13] S. Greulich-Weber, J. R. Niklas, and J. M. Spaeth, J. Phys. C **17**, L911 (1984).
[14] S. Greulich-Weber, J. R. Niklas, E. R. Weber, and J. M. Spaeth, Phys. Rev. B **30**, 6292 (1984).
[15] H. Katayama-Yoshida and A. Zunger, Phys. Rev. Lett. **53**, 1256 (1984).
[16] G. D. Watkins and J. W. Corbett, Phys. Rev. **134**, A1359 (1964).
[17] M. Sprenger, S. H. Muller, and C. A. J. Ammerlaan, Physica **116B**, 224 (1983). The value of g_N mentioned here has been slightly corrected [M. Sprenger (private communication)].
[18] J. Owen and J. H. M. Thornley, Rep. Progr. Phys. (GB) **29**, 675 (1966).
[19] B. di Bartolo, in *Optical Interactions in Solids* (Wiley, New York, 1968).
[20] J. R. Morton and K. F. Preston, J. Magn. Reson. **30**, 577 (1978).